KAT7 / HBO1 is required for the maintenance of leukaemia stem cells.

Laura MacPherson[1,2], Juliana Anokye[1,2], Miriam M. Yeung[1,2], Enid Y. N. Lam[1,2], Yih-Chih Chan[1,2], Chen-Fang Weng[1,2], Paul Yeh[1,2], Kathy Knezevic[1,2], Miriam S. Butler[1,2], Annabelle Hoegl[3], Kah-Lok Chan[1,2], Marian L. Burr[1,2], Linden J. Gearing[4,5], Tracy Willson[4,5], Joy Liu[4], Jarny Choi[4,5], Yuqing Yang[4,5], Rebecca A. Bilardi[4], Hendrik Falk[4,5,6], Nghi Nguyen[7], Paul Stupple[6,7], Thomas S. Peat[6,8], Ming Zhang[4,5,6], Melanie de Silva[4,5,6], Catalina Carrasco-Pozo[6,9], Vicky M. Avery[6,9], Poh Sim Khoo[6,10], Olan Dolezal[6,8], Matthew L. Dennis[6,8], Stewart Nuttall[6,8], Regina Surjadi[6,8], Janet Newman[6,8], Bin Ren[6,8], David J. Leaver[7], Yuxin Sun[7], Jonathan B. Baell[7,11], Oliver Dovey[12], George S. Vassiliou[12], Florian Grebien[13], Sarah-Jane Dawson[1,2,14], Ian P. Street[4,5,6], Brendon J. Monahan[4,5,6], Christopher J. Burns[4,5], Chunaram Choudhary[3], Marnie E. Blewitt[4,5], Anne K. Voss[4,5], Tim Thomas[4,5], Mark A. Dawson[1,2,14,15]

[1]Cancer Research Division, Peter MacCallum Cancer Centre, Melbourne, VIC, Australia
[2]Sir Peter MacCallum Department of Oncology, University of Melbourne, VIC, Australia
[3]Department of Proteomics, The Novo Nordisk Foundation Center for Protein Research, Faculty of Health and Medical Sciences, University of Copenhagen, Copenhagen, Denmark
[4]The Walter and Eliza Hall Institute of Medical Research, Melbourne, VIC, Australia
[5]The Department of Medical Biology, The University of Melbourne, Melbourne, VIC, Australia
[6]Cancer Therapeutics CRC, Parkville, Victoria, Australia.
[7]Medicinal Chemistry Theme, Monash Institute of Pharmaceutical Sciences, Monash University, Melbourne, Victoria, Australia.
[8]Commonwealth Scientific and Industrial Research Organisation (CSIRO), Biomedical Program, Parkville, Victoria, Australia
[9]Discovery Biology, Griffith Institute for Drug Discovery, Griffith University, Nathan, QLD, Australia
[10]Children's Cancer Institute, Kensington, NSW, Australia
[11]School of Pharmaceutical Sciences, Nanjing Tech University, Nanjing, China
[12]Haematological Cancer Genetics, Wellcome Trust Sanger Institute, Hinxton, Cambridge CB10 1SA, UK
[13]Institute for Medical Biochemistry, University of Veterinary Medicine, Vienna, Veterinaerplatz 1, 1210, Vienna, Austria
[14]Centre for Cancer Research, University of Melbourne, VIC, Australia.
[15]Department of Haematology, Peter MacCallum Cancer Centre, Melbourne, VIC, Australia

Corresponding Author:
Professor Mark Dawson
Peter MacCallum Cancer Centre
305 Grattan Street
Melbourne VIC 3000 Australia
Email: Mark.Dawson@petermac.org
Phone: +61 3 8559 7131 / Fax: +61 3 8559 8054

Abstract:

Acute myeloid leukaemia (AML) is a heterogeneous disease characterised by transcriptional dysregulation resulting in a block in differentiation and increased malignant self-renewal. Various epigenetic therapies aimed at reversing these hallmarks of AML have progressed into clinical trials, with most showing modest efficacy due to an inability to effectively eradicate leukaemia stem cells (LSC)[1]. To specifically identify novel dependencies in LSC we screened a bespoke library of small hairpin RNAs (shRNAs) targeting chromatin regulators in a unique *ex vivo* model of LSC. We identified the MYST acetyltransferase HBO1 (KAT7 / MYST2) and several known members of the HBO1 protein complex as critical regulators of LSC maintenance. CRISPR domain screening and quantitative mass spectrometry identified the HBO1 histone acetyltransferase (HAT) domain as being essential to acetylate histone H3K14. H3K14ac facilitates the processivity of RNA polymerase II to maintain the high expression of key genes including *HOXA9* and *HOXA10* that helps sustain the functional properties of LSC. To leverage this dependency therapeutically we developed highly a potent small molecule inhibitor of HBO1 and demonstrate its mode of activity as a competitive analogue of acetyl-CoA. Inhibition of HBO1 phenocopied our genetic data and showed efficacy in a broad range of human cell lines and primary patient AML cells. Together these biological, structural and chemical insights into a novel therapeutic target in AML will enable the clinical translation of these findings.

Manuscript

AML is organized in a loose hierarchy whereby a small population of self-renewing LSC give rise to a large population of more mature leukemic blasts[2]. Whilst several human and mouse AML cell lines have undergone chemical and genetic screens to identify targetable dependencies in this disease[3-5], the majority of these models do not replicate the functional properties of LSC. Analogous to the effective maintenance of embryonic stem cells with therapeutic pressure to decrease differentiation[6], we serendipitously established a method to sustain cells with the transcriptional and functional properties of LSC in liquid culture[7]. Importantly, we concurrently established an isogenic population of AML blasts.

As regulators of transcription are the most frequent mutational targets in AML[8], we performed a pooled negative selection screen with a customized shRNA library against 270 known chromatin modifiers to uncover new transcriptional regulators required for the maintenance of functionally validated LSC[7]. The screen was highly reproducible and clearly identified shared and unique dependencies in LSC and AML blasts (Extended Data Fig. 1a). Interestingly, we observed far fewer dependencies in LSC; with less than one-third of shRNAs depleted in the LSC compared to the blasts (Figure 1a, Supplementary Table 1). We previously showed that the BET bromodomain proteins (BRD2/3/4) were not a major dependency in this LSC model[7] and in addition we found that most of the hitherto identified epigenetic dependencies, including DOT1L, LSD1, EZH2 and PRMT5 that have been the focus of clinical therapies[1] selectively eradicate only the blasts and not the LSC (Extended Data Fig. 1b-c). Of the few dependencies identified in the LSC, we chose to focus on HBO1 as it is not a recognised essential gene and it was equally effective in eradicating the blast and LSC populations (Figure 1a-b and Extended Data Fig. 1d). HBO1 is one of five mammalian members of the highly conserved MYST acetyltransferase family. Recent efforts to identify unique and global genetic dependencies in human cells have highlighted the fact that MOF (KAT8) and TIP60 (KAT5) are pan-essential genes[9], whereas HBO1 is highly expressed in human AML (Extended Data Fig. 2), where it shows a clear and unique dependency[9] (Figure 1 b-c, Extended Data Fig. 3a-b). HBO1 has been reported to function as a major transcriptional regulator primarily via histone acetylation and although various histone modifications have been attributed to HBO1[10-12], these conflicting reports are likely influenced by the specificity of the antibodies used. Therefore, to precisely identify the major histone modifications regulated by HBO1 we coupled conditional deletion of HBO1 in AML cells with quantitative mass spectrometry[13]. These data clearly demonstrate that acetylation of histone H3K14 (H3K14ac) is the major non-redundant chromatin modification mediated by HBO1 (Supplementary Table 2 and Figure 1c).

HBO1, like most HATs can interact with several scaffolding proteins to form functionally distinct catalytically active complexes[14]. Therefore, to identify the major complex members required for the maintenance of LSC we assessed the functional impact of genetic depletion of the HBO1 complex members. We found that knockdown of BRPF2 (BRD1), mEAF6 and PHF16 (JADE3) phenocopied the functional and biochemical effects of HBO1 reduction (Figure 1d-e and Extended Data Fig. 3c). As all of the HBO1 complex components which resulted in impaired maintenance of LSC, also caused a global reduction in H3K14ac, we reasoned that the catalytic domain of HBO1 might be the critical target. CRISPR domain screening with five separate sgRNAs against the MYST domain confirmed that this domain was essential for H3K14ac and LSC survival (Figure 1f-g). While CRISPR domain screening is an effective approach to identify functional domains for drug discovery[15], our rescue experiments with wildtype and catalytically inactive HBO1 provided the highest level of confidence that the HAT domain of HBO1 was the critical therapeutic target in the complex (Figure 1h-i).

The dominant cellular phenotypes that resulted from HBO1 loss included an induction of apoptosis, a prominent G0/G1 cell cycle arrest and a marked differentiation of the immature LSC population (Figure 2a-b, Extended Data Fig. 3d-h). Together these data highlighted the importance of HBO1 in LSC maintenance in an *ex vivo* model system. To address the broader application of our findings in the absence of therapeutic pressure to maintain the LSC state[7], we generated an enriched population of LSC *in vivo*[16] and performed a competition assay to assess the requirement of HBO1 for LSC maintenance *in vivo*. Here we transplanted a fixed ratio of 90% shRNA expressing cells and followed the percentage of shRNA expressing cells contributing to the leukaemia *in vivo*. Despite 90% of HBO1 shRNA expressing LSC being transplanted <5% of them remain at the time of death from leukaemia demonstrating a marked negative selection (Figure 2c). In contrast, both the non-targeting shRNA and shRNA against the closely related MYST family member MOZ (KAT6A) show no detrimental effect to LSC. Similar results were also seen in the NPM1c and FLT3-ITD mouse model[17] (Figure 2d). Moreover, the mice transplanted with HBO1 expressing shRNAs showed a significant survival benefit (Figure 2e, Extended Data Fig. 4a) raising the prospect that HBO1 null LSC are incapable of perpetuating the disease.

To explore this possibility further we generated leukaemias using an Mx1-Cre model for conditional deletion of HBO1 (Extended Data Fig. 4b). The resulting leukaemia was then transplanted into secondary recipient mice and polyinosinic-polycytidylic (pIpC) acid was administered following engraftment. Neither pIpC injection nor heterozygous deletion of HBO1 significantly impact

survival or leukaemia latency (Extended Data Fig. 4c). Leukemic cells derived from *Hbo1*$^{flox/flox}$ *Mx1-Cre* mice show a marked survival advantage and none of the fatal leukaemia that occurred in pIpC treated mice contained complete loss of HBO1 (Figure 2f). In contrast, homozygous deletion of MOZ showed no significant effects in two separate AML mouse models (Extended Data Fig. 4d-f). Together, these data confirm the results from our *ex vivo* model and provide compelling evidence that HBO1 is an essential requirement for LSC maintenance.

To assess the generality of our findings beyond mouse models of AML we chose to delete HBO1 using CRISPR/Cas9 in a range of human AML cell lines encompassing a variety of oncogenic drivers prevalent in AML[8]. We found the majority of AML cell lines recapitulate our results in the murine LSC and show impaired survival of HBO1 deleted cells resulting from an induction of apoptosis, a G0/G1 cell cycle arrest and prominent differentiation (Figure 2g-k, Extended Data Fig. 5). In contrast, very few non-AML cell lines show a similar dependency on HBO1 (Extended Data Fig. 6). Having established the requirement of HBO1 in mouse and human AML models we next wanted to understand the molecular events underpinning its role in LSC maintenance. Consistent with the major cellular phenotype of myeloid differentiation, we found that HBO1 loss results in the marked enrichment of a myeloid differentiation gene expression program (Extended Data Fig. 7a). The established role of HBO1 as a facilitator of transcription led us to examine the top downregulated genes following HBO1 deletion. Interestingly, these downregulated genes are some of the most highly expressed (Extended Data Fig. 7b) and include several homeobox genes (Figure 3a), which are known to be important in LSC maintenance and are commonly upregulated in poor prognosis AML[18]. The requirement of HBO1 to sustain the expression of the essential LSC genes within the 5'-HoxA cluster is conserved in human AML cells (Extended Data Fig. 7c) and the dominant role of these genes in mediating the cellular phenotypes of HBO1 loss is highlighted by the fact that overexpression of *HoxA9* or *HoxA10* significantly rescues the myeloid differentiation and loss of viability observed following HBO1 depletion (Extended Data Fig. 7d-f).

Many of the genes downregulated following HBO1 loss, particularly the homeobox genes, are established targets of both wildtype MLL1 and MLL1-fusion proteins[19]. Using quantitative proteomics in an isogenic leukaemia cell line designed to express a single copy of seven distinct MLL1-fusion proteins,[20] we identified the HBO1 complex functionally required to maintain LSC (Figure 1d) as strong interactors with the N-terminus of MLL1 (Figure 3b-c). Whilst these findings provide molecular insights into how the HBO1 complex is recruited to specific gene loci, to further understand the role of HBO1 in regulating these genes we performed ChIP-Seq analyses for H3K14ac and RNA polymerase-II (RNA POL-II). These data show that H3K14ac deposited by HBO1

is widespread throughout the genome but interestingly at the highly expressed genes repressed by HBO1 loss, H3K14ac and RNA POL-II blanket the entire coding region of the gene (Fig. 3d, Extended Data Fig. 7g). H3K14ac is an evolutionarily conserved histone modification and recent evidence suggests that H3K14ac may regulate transcriptional elongation[21]. Consistent with this, we find markedly increased RNA POL-II levels within the coding region of highly expressed genes containing the highest H3K14ac levels (Fig. 3e). Furthermore, expressed genes with the highest level of H3K14ac have the lowest RNA POL-II travelling ratio and HBO1 loss leads to a more prominent loss of RNA POL-II within the body these genes (Fig. 3f, Extended Data Fig. 7h). The processivity of RNA POL-II is greatly facilitated by chromatin remodelling complexes and H3K14ac has been shown to be specifically bound by SMARCA4[22], DPF2[23] and several members of the ISWI family where it markedly potentiates their remodelling activity[24]. Remarkably, these chromatin remodelling complex members show a similar cancer cell line dependency profile to HBO1 with a predilection for AML[9] and also phenocopy the effects of HBO1 loss in LSC (Fig. 3g-i, Extended Data Fig. 7i).

Our genetic data in both mouse and human AML clearly identified the catalytic activity of HBO1 as the central therapeutic target. A long-standing challenge in the field has been the ability to develop highly selective small molecule HAT inhibitors that discriminate between the major families of histone acetyltransferases. We have recently demonstrated that the acylsulfonylhydrazide backbone provides a simple chemical scaffold for the generation of selective MYST-family inhibitors[25]. Using this template, we generated WM-3835 (N'-(4-fluoro-5-methyl-[1,1'-biphenyl]-3-carbonyl)-3-hydroxybenzenesulfonohydrazide; Figure 4a), which retains specificity for the MYST acetyltransferases but has increased potency against HBO1 compared to WM-1119 (Figure 4b and Extended Data Fig. 8a). Crystal structure of HBO1 with WM-3835 bound in the acetyl-CoA binding site was solved to 2.14 Å (Figure 4c, Extended Data Fig. 9). Overlay of this crystal structure with WM-1119 in MYST$^{Cryst\ 25}$ shows that WM-3835 makes additional interactions with the protein surface, which may explain the increased activity of WM-3835 against HBO1. Specifically, the WM-3835 phenol forms a hydrogen-bonding network to Glu525 and Lys488, neither of which is conserved throughout the MYST family.

WM-3835 is a cell permeable small molecule that results in a rapid and selective reduction in H3K14ac levels (Figure 4d). Treatment of a diverse set of AML cell lines with WM-3835 resulted in a marked reduction in tumour cell viability (Figure 4e, Extended Data Fig. 10a) that was not observed following treatment with the inactive analogue WM-2474[25] (Extended Data Fig. 8b). Notably, we observed an excellent dose-response relationship between a reduction of H3K14ac and cell viability (Extended Fig. 8c-d). Although WM-3835 retains

potency against MOZ and QKF/MORF (KAT6B), CRISPR/CAS9 mediated deletion of these enzymes do not alter the activity of WM-3835 (Figure 4f), highlighting that the efficacy of WM-3835 in AML is primarily via HBO1 inhibition. Moreover, treatment of cells with WM-3835 phenocopied the molecular and cellular effects of genetic depletion of HBO1 by inducing apoptosis, a G0/G1 cell cycle arrest, differentiation of human AML cells and transcriptional repression on *HOXA9* and *HOXA10* (Figure 4g-I, Extended Data Fig. 8e-h). Similar to our genetic studies, overexpression of *HoxA9* and *HoxA10* ameliorated the effects of WM-3835 (Extended Data Fig. 8i). Although the rapid metabolism, including glucuronidation of WM-3835 precluded efficacy experiments *in vivo* (Extended Data Fig. 10b-c), the compound showed a prominent reduction of clonogenic potential in primary human AML cells derived from several patients harbouring different driver mutations, highlighting the therapeutic potential of catalytic inhibitors against HBO1 in AML (Figure 4j).

Central to the ambition to alter the natural history of AML is the requirement for new therapies that effectively target LSC from the outset. LSC serve as the reservoir for evolving resistance to conventional and targeted therapies and our clinical experience has clearly proven that monotherapies are incapable to subvert the vast adaptive potential of LSC. Therefore, the future lies in identifying key therapeutic targets in LSC that can be leveraged in combination with other effective agents including conventional chemotherapy. Here we identify HBO1 as a targetable dependency in LSC. Our molecular insights suggest that MLL1 recruits HBO1 to regulate highly expressed LSC genes including the HOXA cluster through H3K14ac, which potentiates the activity of specific chromatin remodelling complexes enabling greater processivity of RNA POL-II (Figure 4k). The blueprint for selective and potent inhibition of HBO1, together with these new biological insights provide the impetus and platform for the translation of these findings into the clinical setting.

ACKNOWLEDGEMENTS

We thank Drs. Carrie Lovitt and Joshua Wingerd and Susan Jackson and Elizabeth Allan for their technical contributions to this project. The work in the Dawson, Blewitt and Burns laboratories was supported by the Cancer Council Victoria Venture Grant Scheme and Dawson lab work from project grant funding from the National Health and Medical Research Council of Australia (1085015). We thank the following funders for fellowship and grant support: Leukaemia Foundation Australia senior fellowship, Cancer Council Victoria Dunlop Fellopship and Howard Hughes Medical Institute international research scholarship (M.A.D); Victoria Cancer Agency early-career (L.M) and mid-career (E.Y.N.L) fellowships; CSL Centenary fellowship (S.J.D), Snowdome Foundation (P.Y) and Maddie Riewoldt's Vision Foundation (Y.C.C) and Bellberry-Viertel Senior Medical Research Fellowship (M.E.B), Novo Nordisk Foundation Hallas Møller Fellowship NNF14OC0008541 (C.C.), National Health and Medical Research Council of Australia through project grants 1081421 (J.B.B, T.T), 575558, 1084248 (A.K.V, T.T), research fellowship 1081421 (A.K.V) and postgraduate scholarship (K-L. C). Salary support for M.Z and M.D.S, H.F, C.C, P.S.K, P.S, I.P.S and B.J.M was provided by the Cancer Therapeutics CRC funded through the Australian Government's Cooperative Research Centre programme. The Novo Nordisk Foundation Center for Protein Research is supported financially by the Novo Nordisk Foundation (Grant agreement: NNF14CC0001). This work was made possible through the Victorian State Government Operation Infrastructure Support and Australian National Health and the Medical Research Council Research Institute Infrastructure Support Scheme. We thank the Australian Synchrotron and beamline scientists for help with data collection; this research was undertaken in part using the MX2 beamline at the Australian Synchrotron and made use of the ACRF detector.

AUTHOR CONTRIBUTIONS

M.A.D developed the overall concept behind the study and supervised the project with important advice from L.M, M.E.B, C.J.B, A.K.V, T.T, C.C, F.G and B.J.M. The manuscript was written by L.M, B.J.M and M.A.D with input from all the authors. L.M performed the majority of the experiments with help from J.A, E.Y.N.L, Y-C.C, C-F.W, M.M.Y, P.Y, K-L. C, K.K, M.S.B, M.L.B, J.L, Y.Y, A.D, R.A.B, T.T, H.F, M.D.S, N.N, P.S.K, M.Z and V.M.A and C.C-P. Critical reagents and interpretation of the research findings were provided by A.K.V, F.G, S-J.D, P.S, T.S.P, J.B.B, T.T, O.D, G.S.V, C.C and I.P.S. The shRNA library was designed and built by L.J.G, T.W, J.l, J.C and M.E.B. A.H. and C.C. performed mass spectrometry analysis of histone acetylation sites. Protein production, SPR and structural studies were done by

S.N, R.S, M.L.D, O.D, R.S, J.N, B.R and T.S.P. WM-3835 was developed by J.B.B, D.J.L, and N.N with analytical support by Y.S.

COMPETING INTERESTS

M.A.D. has been a member of advisory boards for CTX CRC, Storm Therapeutics, Celgene and Cambridge Epigenetix. The Dawson lab receives research funding from Pfizer. The remaining authors declare no competing financial interests.

References:

1. Dawson, M.A. The cancer epigenome: Concepts, challenges, and therapeutic opportunities. *Science* **355**, 1147-1152 (2017).
2. Thomas, D. & Majeti, R. Biology and relevance of human acute myeloid leukemia stem cells. *Blood* **129**, 1577-1585 (2017).
3. Wang, T. *et al.* Gene Essentiality Profiling Reveals Gene Networks and Synthetic Lethal Interactions with Oncogenic Ras. *Cell* **168**, 890-903 e15 (2017).
4. Tzelepis, K. *et al.* A CRISPR Dropout Screen Identifies Genetic Vulnerabilities and Therapeutic Targets in Acute Myeloid Leukemia. *Cell Rep* **17**, 1193-1205 (2016).
5. Zuber, J. *et al.* RNAi screen identifies Brd4 as a therapeutic target in acute myeloid leukaemia. *Nature* **478**, 524-8 (2011).
6. Ying, Q.L. *et al.* The ground state of embryonic stem cell self-renewal. *Nature* **453**, 519-23 (2008).
7. Fong, C.Y. *et al.* BET inhibitor resistance emerges from leukaemia stem cells. *Nature* **525**, 538-42 (2015).
8. Grimwade, D., Ivey, A. & Huntly, B.J. Molecular landscape of acute myeloid leukemia in younger adults and its clinical relevance. *Blood* **127**, 29-41 (2016).
9. Tsherniak, A. *et al.* Defining a Cancer Dependency Map. *Cell* **170**, 564-576 e16 (2017).
10. Kueh, A.J., Dixon, M.P., Voss, A.K. & Thomas, T. HBO1 is required for H3K14 acetylation and normal transcriptional activity during embryonic development. *Mol Cell Biol* **31**, 845-60 (2011).
11. Doyon, Y. *et al.* ING tumor suppressor proteins are critical regulators of chromatin acetylation required for genome expression and perpetuation. *Mol Cell* **21**, 51-64 (2006).
12. Sauer, T. *et al.* MYST2 acetyltransferase expression and Histone H4 Lysine acetylation are suppressed in AML. *Exp Hematol* **43**, 794-802 e4 (2015).
13. Weinert, B.T. *et al.* Time-Resolved Analysis Reveals Rapid Dynamics and Broad Scope of the CBP/p300 Acetylome. *Cell* **174**, 231-244 e12 (2018).
14. Saksouk, N. *et al.* HBO1 HAT complexes target chromatin throughout gene coding regions via multiple PHD finger interactions with histone H3 tail. *Mol Cell* **33**, 257-65 (2009).
15. Shi, J. *et al.* Discovery of cancer drug targets by CRISPR-Cas9 screening of protein domains. *Nat Biotechnol* **33**, 661-7 (2015).
16. Krivtsov, A.V. *et al.* Transformation from committed progenitor to leukaemia stem cell initiated by MLL-AF9. *Nature* **442**, 818-22 (2006).
17. Mupo, A. *et al.* A powerful molecular synergy between mutant Nucleophosmin and Flt3-ITD drives acute myeloid leukemia in mice. *Leukemia* **27**, 1917-20 (2013).
18. Alharbi, R.A., Pettengell, R., Pandha, H.S. & Morgan, R. The role of HOX genes in normal hematopoiesis and acute leukemia. *Leukemia* **27**, 1000-8 (2013).
19. Ballabio, E. & Milne, T.A. Epigenetic control of gene expression in leukemogenesis: Cooperation between wild type MLL and MLL fusion proteins. *Molecular & Cellular Oncology* **1**, e955330 (2014).

20. Skucha, A. *et al.* MLL-fusion-driven leukemia requires SETD2 to safeguard genomic integrity. *Nat Commun* **9**, 1983 (2018).
21. Church, M., Smith, K.C., Alhussain, M.M., Pennings, S. & Fleming, A.B. Sas3 and Ada2(Gcn5)-dependent histone H3 acetylation is required for transcription elongation at the de-repressed FLO1 gene. *Nucleic Acids Res* **45**, 4413-4430 (2017).
22. Shen, W. *et al.* Solution structure of human Brg1 bromodomain and its specific binding to acetylated histone tails. *Biochemistry* **46**, 2100-10 (2007).
23. Huber, F.M. *et al.* Histone-binding of DPF2 mediates its repressive role in myeloid differentiation. *Proc Natl Acad Sci U S A* **114**, 6016-6021 (2017).
24. Dann, G.P. *et al.* ISWI chromatin remodellers sense nucleosome modifications to determine substrate preference. *Nature* **548**, 607-611 (2017).
25. Baell, J.B. *et al.* Inhibitors of histone acetyltransferases KAT6A/B induce senescence and arrest tumour growth. *Nature* **560**, 253-257 (2018).

Figure Legends

Figure 1: HBO1 is an essential dependency in LSC.

a. Pooled negative-selection screening in MLL-AF9 bulk blasts (left) and leukaemic stem cells (LSC, right). Volcano plot depicting changes in representation of shRNAs in the screen between days 2 and 14. One dot represents the mean of two independent experiments for each gene. **b.** Negative selection competition assays depicting the percentage of shRNA over time in blasts and LSC expressing *Hbo1* shRNAs. n=3 (mean + s.e.m.). **c.** Immunoblot of HBO1, H3K14Ac and H3K27Ac n=3 and **d.** Negative selection competition assays n=3 (mean + s.e.m.) and **e.** Immunoblot of H3K14ac in LSC expressing shRNAs targeting Hbo1 complex members. n=3. **f.** Negative selection competition assays n=3 (mean + s.e.m.) and **g.** Immunoblot of HBO1, H3K14Ac and H3K27Ac in LSC expressing Cas9 and sgRNAs against Rosa26 (control) or the *Hbo1* catalytic domain. n=3. **h.** Schematic outline of Hbo1 rescue experiments. Wildtype (wt) or catalytic mutant *Hbo1* (E508Q) resistant to sgHbo1 e12.2 or GFP were overexpressed in LSC expressing Cas9 and then transduced with sgRNAs targeting *Hbo1*. **i.** Hbo1 rescue negative selection competition assays. n=3 (mean + s.e.m.). sgHbo1 e11.1 targets endogenous (END) and overexpressed (OE) *Hbo1*. Right panel: immunoblot of overexpressed wildtype and catalytic mutant HBO1.

Figure 2: Loss of HBO1 impairs LSC maintenance *in vivo*.

a. Cell cycle profile n=3 (mean + s.e.m.) and **b.** Surface expression of Gr1 and CD11b in LSC expressing Cas9 transduced with Hbo1 sgRNAs. n=3. **c.** Percentage of shRNA positive cells in bone marrow (BM) and spleen (SP) at endpoint in recipients transplanted with 5° MLL-AF9 cells. (mean ±s.d.) n= 5/group. **d.** Percentage of shRNA positive cells (mean ±s.e.m.) in bone marrow (BM) at endpoint in recipients transplanted with 3° NPM1c/FLT3-ITD cells. n=6/group. **e.** Kaplan-Meier curves of recipients injected with NPM1c/FLT3-ITD cells expressing hairpins targeting *Hbo1*. n=5/group. Inset: immunoblot of HBO1 in NPM1c/FLT3-ITD cells expressing Hbo1 hairpin from a recipient that died showed that the hairpin was inactivated. Hbo1 levels from parental NPM1c/FLT3-ITD cells are shown for comparison. **f.** Kaplan-Meier curves of C57BL/6 mice injected with 10^3 *Hbo1*$^{flox/flox}$ *Mx1-Cre* 1° MLL-AF9 leukaemic cells. Mice were treated with saline or pIpC (arrowheads). Inset: representative genotyping of recipient bone marrow at endpoint. n=6/group. **g.** Negative selection competition assays n=3 (mean + s.e.m.) and **h.** Immunoblot of HBO1 and H3K14Ac n=3. and **i.** Cell cycle profile n=3 (mean + s.e.m.) and **j.** Apoptosis n=3 (mean + s.e.m.). and **k.** Surface expression of CD11b in Molm13 cells expressing Cas9 and HBO1 sgRNAs. n=3.

Figure 3: HBO1 regulates expression of the 5' end of the HoxA cluster in AML.

a. Heat map depicting normalised expression of the top 25 down-regulated genes in LSC with HBO1 loss. **b.** Heat map displaying the mean spectral counts from AP-MS data of 7 MLL1 translocation partners for all MYST family members. **c.** Network analysis of known protein interaction partners of HBO1 (thick grey lines) linking to known members of the HBO1 complex and HBO1 network to 7 MLL-fusions (thin red line). Nodes size represents the mean spectral counts for each interaction. Node border width is scaled to the number of interactions with the MLL-fusions. **d.** ChIP-seq profiles of H3K14Ac and RNA Polymerase II (RNA POL-II) at *HOXA* gene cluster in LSC expressing Cas9 and Hbo1 sgRNA. Representative of n=3 biological replicates. **e.** RNA POLII coverage across highly expressed genes (high) divided according to H3K14ac levels. **f.** Waterfall plots of change in RNA POLII (POL-II LFC) binding throughout the gene promoter (-30 to +300 bp) and gene body (+300 bp to TES) following HBO1 loss for highly expressed genes divided according to H3K14ac levels. **g.** Negative selection competition assays n=3 (mean + s.e.m.) and **h.** *Hoxa9* and *Hoxa10* mRNA expression in LSC expressing Cas9 and *Smarca4, Dpf2* or *Smarca5* sgRNAs. n=3 (mean + s.e.m.) **i.** Surface expression of Gr1 and CD11b in LSC expressing Cas9 and Dpf2 sgRNAs. n=2.

Figure 4: Treatment with WM-3835 reduces AML growth.

a. Chemical structure of WM-3835. **b.** Selectivity and potency profile of WM-3835 and WM-1119 superimposed on the KAT family dendrogram as measured by histone acetyltransferase inhibition assay. Values listed in Extended Data Figure 8A. **c.** Ribbon representation of the HBO1-BPRF2 crystal structure(cyan) with WM-3835 bound (yellow with element colouring; PDB code 6MAJ) overlaid with the corresponding region of $MYST^{CRYST}$ with WM-1119 bound (magenta with element colouring; PDB code 6BA4), where non-conserved residues of $MYST^{CRYST}$ are shown in (blue). Key residues highlighted show hydrogen bond with the phenol of WM-3935 **d.** Immunoblot of H3K14Ac in LSC treated with WM-3835. n=2. **e.** LSC and human AML cell proliferation with 1 μM WM-3835. n=3 (mean + s.e.m.). **f.** LSC with *Moz* or *Qkf/Morf* deletion proliferation with WM-3835 n=3 (mean± s.e.m.). Right, immunoblot of H3K23ac and H3K14ac in LSC with *Moz* or *Qkf/Morf* deletion. n=2. **g.** Cell cycle profile n=3 (mean + s.e.m.) and **h.** Surface expression of CD11b in Molm13 cells with WM-3835. n=3. **i.** *Hoxa9* expression in murine LSC and Molm13 cells with WM-3835. n=2. **j.** Clonogenic assays with primary patient AML cells treated with WM-3835. n=5 (mean + s.e.m.). **k.** Schematic overview of AML gene regulation by the HBO1 complex.

Extended Data Figure Legends

Extended Data Figure 1. Hbo1 is an AML specific dependency.

a. RNAi screen multidimensional scaling plot of shRNA sequences from bulk leukaemic blasts (bulk) and leukaemic stem cells (LSC) over 14 days of screening. Screens were performed in duplicate (R1 and R2). **b.** Ezh2, Lsd1 and Prmt5 mRNA expression relative to non-targeting (NT) in LSC expressing shRNAs. Validation of the shRNA's against DOT1L have previously been published[26]. n=3 (mean + s.e.m.) **c.** Negative selection competition assays in bulk leukaemic blast and LSC expressing shRNAs against Ezh2, Lsd1 and Prmt5. n=3 (mean + s.e.m.). **d.** Hbo1 mRNA expression relative to non-targeting (NT) in LSC expressing shRNAs. n=3 (mean + s.e.m.).

Extended Data Figure 2. Expression levels of HBO1.

a. Box plot of HBO1 expression levels in different cancer types from TCGA[27]. The upper limit, centre and lower limit of each box denotes the upper quartile, median and lower quartile of the data respectively **b.** Dot plot of HBO1 expression levels in normal haematopoietic and AML cells from BloodSpot[28], line indicates mean expression.

Extended Data Figure 3. Hbo1 depletion increases apoptosis, cell cycle arrest and myeloid differentiation in murine LSC.

a. Negative selection competition assays in LSC expressing shRNA's against *Moz*, *Qkf* or *Hbo1*. n=3 (mean + s.e.m.). **b.** Negative selection competition assays in LSC expressing Cas9 transduced with sgRNAs targeting *Moz* or *Qkf*. n=3 (mean + s.e.m.). **c.** Hbo1 complex member expression relative to non-targeting (NT) in LSC expressing shRNAs targeting individual complex members. n=3 (mean + s.e.m.) **d.** Apoptosis of LSC expressing shRNAs targeting *Hbo1*. n=3 (mean + s.e.m.). **e.** Cell cycle profile of LSC expressing shRNAs targeting *Hbo1*. n=3 (mean + s.e.m.). **f.** Surface expression of Gr1 and CD11b in LSC expressing shRNAs against Hbo1. n=3. **g.** Apoptosis of LSC expressing Cas9 and sgRNAs targeting *Hbo1*. n=3 (mean + s.e.m.). **h.** Surface expression of cKit (CD117) in LSC expressing sgRNAs targeting *Hbo1*. Representative of n=2 biological replicates.

Extended Data Figure 4. *in vivo* depletion of Hbo1 increases disease latency.

a. Kaplan-Meier curves of NSG mice transplanted with quinary MLL-AF9 leukaemic cells expressing shRNAs targeting Hbo1 and Moz. n=6 per group. **b.** Schematic of wildtype and *Hbo1* mutant alleles with numbered black boxes representing exons. Genotyping primers are indicated (adapted from Kueh et., al). **c.** Kaplan-Meier curves of C57BL/6 mice injected with 10^6 *Hbo1* $^{flox/+}$ *Mx1-Cre* primary MLL-AF9 leukaemic cells. Mice were treated with saline or pIpC. n=12 per group. Right: representative genotyping of recipient bone marrow at endpoint. **d.** Kaplan-Meier curves of C57BL/6 mice injected with *Moz*$^{+/+}$, *Moz*$^{+/-}$ or

Moz$^{-/-}$ MLL-AF9 leukaemic cells. n=5 per group. **e.** Kaplan-Meier curves of Balb/c mice injected with *Moz*$^{+/+}$ *or Moz*$^{-/-}$ HoxA9/Meis1 leukaemic cells. n = 5 per group.

Extended Data Figure 5. HBO1 is a dependency in various AML subtypes.

a. Negative selection competition assays in human AML cell lines expressing Cas9 and sgRNAs targeting *HBO1*. n=3 (mean + s.e.m.). Driver mutations are in parentheses. **b.** Immunoblot of HBO1 and H3K14Ac in OCI-AML3 cells expressing Cas9 and sgRNAs targeting *HBO1*. n=3 (mean + s.e.m.). **c.** Cell cycle profile of OCI-AML3 cells expressing Cas9 and sgRNAs targeting HBO1. n=3 (mean + s.e.m.). **d.** Apoptosis of OCI-AML3 cells expressing Cas9 and sgRNAs targeting *HBO1*. n=3 (mean + s.e.m.). **e.** Surface expression of CD11b in OCI-AML3 cells expressing Cas9 and sgRNAs targeting *HBO1*. n=3.

Extended Data Figure 6. HBO1 dependency in other cancers.

Negative selection competition assays in human cancer cell lines expressing Cas9 and sgRNAs targeting *HBO1*. n=3 (mean + s.e.m.). Cancer type is in parentheses.

Extended Data Figure 7. Hbo1 depletion increases myeloid signature and decreases global H3K14Ac

a. Barcode plot evaluating changes in myeloid development signature following HBO1 depletion with sgHbo1 e11.1 and e12.2 in LSC. n=3. **b.** Bar plot of changes in genes expression following HBO1 deletion in LSC ranked by expression levels. Green bars show the top 25 most down-regulated genes following *Hbo1* deletion. **c.** HOXA9 and HOXA10 mRNA expression in Molm13 and OCI-AML3 cells expressing Cas9 and sgRNA targeting *HBO1*. n=3 (mean ± s.e.m.). **d.** Surface expression of CD11b in LSC overexpressing *Hoxa9* or *Hoxa10* and sgRNAs targeting Hbo1. **e.** Immunoblot of overexpressed Hoxa9 or Hoxa10 in LSC cells expressing Cas9. Representative of n=3 biological replicates. **f.** *Hoxa9* and *Hoxa10* rescue negative selection competition assays. Representative of n=3 biological replicates. **g.** ChIP-seq profiles of H3K14ac and RNA Polymerase II (RNA POL-II) at the *Pbx3* locus in LSC expressing Cas9 and an sgRNA targeting *Hbo1*. Representative of n=3 biological replicates. **h.** RNA PolII traveling ratio distribution for highly expressed genes divided according to H3K14ac levels from ChIP-seq. **i.** Surface expression of Gr1 in LSC overexpressing sgRNAs targeting *Smarca5*. Representative of n=3 biological replicates.

Extended Data Figure 8. WM-3835 inhibits cell growth and *HOXA* expression in AML.

a. KAT biochemical and SPR values for WM-3835 compared to WM-1119. Biochemical assay was done at 1 μM acetyl-CoA, K_m of HBO1. **b.** Proliferation assays of human AML cells treated with 1 μM WM-2474. n=3 (mean + s.e.m.) **c.**

Cellular H3K14Ac biomarker assay dose response curves for WM-3835 (blue) and WM-1119 (red) (mean ± s.e.m.). n=6 **d.** Growth inhibition assays of MLL-AF9 AML cell line Molm13 treated with WM-3835 at doses indicated. Boxes represent minimum and maximum values. n=11 (mean ± s.e.m.) **e.** Cell cycle profile of OCI-AML3 cells treated with WM-3835 or vehicle. n=3 (mean + s.e.m.) **f.** Apoptosis of OCI-AML3 cells treated with WM-3835 or vehicle. n=3 (mean + s.e.m.). **g.** Surface expression of CD11b in OCI-AML3 cells treated with WM-3835 or vehicle. n=3 **h.** *HOXA10* mRNA expression in LSC and Molm13 cells treated with WM-3835 or vehicle. n=3 (mean + s.e.m.) **i.** *HOXA9* and *HOXA10* mRNA expression in OCI-AML3 cells treated with WM-3835. n=3 (mean + s.e.m.). **j.** *Hoxa9* and *Hoxa10* rescue proliferation assays with 1 μM WM-3835 in LSC. n=3 (mean ± s.e.m.).

Extended Data Figure 9. HBO1 Crystal Structure.

a. Data collection and refinement statistics of WM-3835 HBO1-BRPF2 co-crystal structure. **b.** WM-3835 binding site in HBO1-BRPF2. WM-3835 shown in silver with element colouring and the OMIT electron density map contoured to 3 σ shown in green. **c.** Overlay of WM-3835 and acetyl-coA (purple with element colouring), showing that WM-3835 binds in the acetyl-coA binding site of HBO1. **d.** Ribbon diagram of HBO1-BRPF2 showing WM-3835 bound to the acetyl-coA binding site. **e.** Space filling model showing WM-3835 (yellow with element colouring) in the acetyl-coA binding pocket of HBO1-BRPF2.

Extended Data Figure 10. High *in vitro* metabolism and poor *in vivo* oral exposure of WM-3835.

a. Proliferation assays of human AML cell lines treated with 1 μM WM-3835. **b.** WM-3835 demonstrates high clearance in both human and mouse liver microsome assays. The use of dual cofactors (UDPGA and NADPH) results in an increased rate of clearance in human liver microsomes, which is consistent with glucuronidation having a role in the clearance of this compound. **c.** BALB/c female mice were dosed with WM-3835 at 100 mg/kg *p.o. b.i.d.* formulated in 20% PEG400/10% Solutol or vehicle. 4 hours after the third dose blood samples were collected. An average total drug concentration of 1860 nM was observed. The free drug level was determined to be 2.6 nM after accounting for mouse plasma protein binding (fu 0.0014). This free drug level was considered too low to affect H3K14 acetylation based on the *in vitro* H3K14ac cellular biomarker data (Figure 4). An additional chromatographic peak eluting earlier than WM-3835 was detected in the plasma samples from the treatment group. Subsequent analyses using predicted multiple-reaction monitoring and accurate mass measurement indicated that it is likely to be a glucuronide conjugate of WM-3835, consistent with the *in vitro* metabolism data.

Methods

Cell Culture

MLL-AF9 bulk blasts and LSC were generated as previously described[7]. Murine and human cell lines (NOMO-1, Molm13, MV4;11, HL-60, OCI-M2, OCI-AML3, K562, NB4, SKM-1, and KG-1) were maintained in RPMI-1640 supplemented with 10% FCS, 2 mM GlutaMAX, 100 IU ml^{-1} penicillin, 100 ug ml^{-1} streptomycin under standard culture conditions (5% CO_2, 37°C). Blasts and LSC were maintained in the presence of 0.1% DMSO or 1 μM I-BET151, respectively, and IL-3 (10 ng ml^{-1}). HEK293T cells were maintained in DMEM supplemented with 10% FCS, 100 IU ml^{-1} penicillin, 100 ug ml^{-1} streptomycin in 10% CO_2 at 37°C. All cell lines were regularly tested and verified to be mycoplasma negative by PCR analysis by in-house genotyping. Human cell lines were authenticated by STR profiling through the Australian Genome Research Facility (Melbourne, Victoria).

Virus production and transduction

Retrovirus was produced by triple transfection of HEK293T cells with a retroviral LMP-BFP transfer vector and structural pMD1-gag-pol plasmid and Vsv-g envelope plasmid at a 0.75:0.22:0.03 ratio, as previously described[29]. Lentivirus was produced by triple transfection of HEK293T cells with a lentiviral transfer vector, and the packaging plasmids psPAX2 and Vsv-g at a 0.5:0.35:15 ratio. All transfections were performed using polyethylenimine (PEI). Viral supernatants were collected 48 h following transfection, filtered through a 0.45 μm filter and added to target cells.

To examine the effect of loss of MOZ function on progression of leukaemia foetal liver cells were isolated from E13 embryos with a germline deletion of *Moz* or littermate controls[30]. E13 embryos were used because *Moz* null embryos die by E14. Foetal liver cells (C57B/6; CD45.2 cell surface phenotype) were transfected with MSCV expressing either MLL-AFP and GFP or Meis1, Hoxa9 and GFP or control viruses: empty vector (Gfp) or Meis1-Gfp or Hoxa9-Gfp alone (not shown); prepared for infection as above except the ECO envelope protein was used. After overnight culture infected foetal liver cells were injected into C57B/6 CD45.1 recipient mice, which had been irradiated with a single dose of 700 rads.

Pooled negative-selection RNAi screening

A custom shRNA library targeting 270 murine epigenetic enzymatic genes was designed using the Designer of Small Interfering RNA Website and subcloned into the LMP-blue fluorescent protein (BFP) vector with selectable markers EBFP/puromycin as previously described[31]. After sequence verification, 1922 shRNAs (6-8 per gene) were combined with several positive- and negative control shRNAs at equal concentration in one pool. This pool was used to produce retrovirus, which was then transduced into 4 x 10^6 MLL-AF9 bulk blasts

and LSC at a multiplicity of infection of 0.3 and selected with 3 and 5 μg ml^{-1} puromycin, respectively, commencing 30 h after transduction. Throughout 14 days of puromycin selection more than 20 million cells were maintained at each passage to preserve 10 000-fold library representation. Genomic DNA from D2 to D14 was isolated (DNeasy Blood & Tissue Kit, Qiagen) from both blasts and LSC. shRNA sequences were amplified by PCR with primers containing adaptors for Illumina sequencing as previously described[32]. The resulting libraries were sequenced with single-end 50 bp reads on a HiSeq2500. The shRNA sequences were mapped to the shRNAs within the pool, and the shRNA counts were analysed as previously described[33]. The likelihood ratio test was used to determine the hairpins significantly depleted over the timecourse of the experiment. Genes with at least two hairpins depleted by greater than 10-fold were considered to be significant dependencies.

CRISPR-Cas9-mediated gene disruption

sgRNA oligonucleotides (Sigma-Aldrich) were phosphorylated, annealed and cloned into lentiviral expression vectors, pKLV-U6gRNA(BbsI)-PGKpuro2ABFP (Addgene 50946, deposited by K. Yusa). Cells were first transduced with the FUCas9Cherry (Addgene 70182, deposited by M. Herold) and FACS sorted for high mCherry expression and then subsequently transduced with the pKLV sgRNA expression vector.

shRNA and sgRNA Competitive Proliferation Assay

Bulk blast and LSC were transduced with retrovirus expressing a gene specific shRNA and the percentage of BFP-positive cells was measured between days 1 and 13 post-transduction and normalised to the percentage of BFP positive cells at day 1. For sgRNA, Cas9-expressing cells were transduced with a lentivirus expressing an *Hbo1* sgRNA and the percentage of double positive BFP and mCherry cells was measured between days 2 and 14 post-transduction and normalised to the percentage BFP/mCherry positive cells at day 2 or 4. All shRNA and sgRNA sequences are provided in Supplementary Table 3.

Antibodies

Immunoblotting: rabbit anti-acetyl-histone H3 (Lys 14) (D4B9, Cell Signalling Technology), mouse anti-histone H3K14Ac (13HH3-1A5, Active Motif), rabbit anti-histone H3 (acetyl K27) (ab4729, Abcam), rabbit anti-KAT7/Hbo1/MYST2 (ab70183, Abcam), rabbit anti-histone H3 (ab1791, Abcam), mouse anti-HSP60 (C10, Santa Cruz), rabbit anti-HSP60 (H-300, Santa Cruz), mouse anti-FLAG (M2, Sigma), mouse anti-RNA polymerase II (CTD4H8, Millipore). Flow Cytometry: Alexa Fluor 700 anti-Gr1 (108422, BioLegend) and Brilliant Violet 605 anti-CD11b (101237, Biolegend), APC/Cy7 anti-mouse CD117 (c-kit) (313228, Biolegend).

Flow Cytometry

Cell apoptosis, hairpin or sgRNA positive cells were washed once with PBS and assessed using FITC conjugated Annexin V (640906, Biolegend) and DAPI (D9542, Sigma) staining according to manufacturer's instructions. For cell cycle analysis, hairpin or sgRNA positive cells were washed with PBS and fixed for at least 2 hours at -20°C in 70% ethanol. Fixed cells were PBS washed and incubated at 4°C in 4',6-diamidino-2-phenylindole (DAPI) staining solution (1 mg ml^{-1} DAPI, 0.05% (v/v) Triton X-100 in PBS) for 30 min. For surface expression of myeloid markers, hairpin or sgRNA positive cells were washed in PBS and stained for Gr1 or CD11b on ice for 30 min in PBS plus 5% FCS. All flow cytometry analyses were performed on a LSR Fortessa X-20 flow cytometer (BD Biosciences) and all data analysed with FlowJo. Cell sorting was performed on a FACSAria Fusion 5 (BD Biosciences).

Immunoblotting

Hairpin or sgRNA positive cells were lysed in 20 mM HEPES pH7.9, 0.5 mM EDTA, 2% SDS plus 1X protease inhibitor cocktail (Roche) by brief sonication. Lysates were heated to 95°C in SDS sample buffer with 50 mM DTT for 5 min, separated by SDS-PAGE and transferred to PVDF membrane (Millipore). Membranes were blocked in 5% milk in TBS +0.1% Tween-20, probed with the indicated antibodies, and reactive bands visualised using ECL Prime (GE).

Analysis of HBO1-regulated acetylation of core histones

Murine MLL-AF9 *CreERT2 Hbo1$^{fl/fl}$* conditional knockout cells were SILAC-labelled with "light" ($^{12}C_6$,$^{14}N_4$-arginine and $^{12}C_6$,$^{14}N_2$-lysine) and "heavy" (($^{13}C_6$,$^{15}N_4$-arginine and $^{13}C_6$,$^{15}N_2$-lysine, Cambridge Isotope Laboratories). To delete HBO1, the heavy-labelled cells were treated with 4-hydroxytamoxifen (200 nM) for ~40 hours, and light-labelled control cells were treated with vehicle control. Histones were extracted as described previously.[34] Briefly, cells were lysed mechanically in ice-cold hypotonic lysis buffer (10 mM Tris pH 8.0, 1 mM KCl, 1.5 mM $MgCl_2$, 1 mM DTT and 1× complete protease inhibitor cocktail (Roche)) and intact nuclei were harvested by centrifugation. Histones were acid-extracted with H_2SO_4 (0.4 N) and precipitated with TCA (33% final concentration). Purified histones from knockout and control cells were mixed in equal amounts, separated on SDS-PAGE, in-gel digested with Trypsin or LysC. (Sigma). The histone peptides were analysed by online nanoflow liquid chromatography coupled tandem mass spectrometry (LC-MS/MS) using a Proxeon easy nLC system connected to a Q-Exactive HFX mass spectrometer (Thermo Scientific). The raw data was computationally processed using MaxQuant[35] (Version 1.5.6.5) and searched against the UniProt database (downloaded Jan 23, 2014) using the integrated Andromeda search engine (http://www.maxquant.org/). The data were searched with: 3 missed cleavages,

minimum peptide length of 6 amino acids, re-quantify option selected, acetylation was included as variable modification.

Rescue Assays

cDNA of *Hbo1* and *Hoxa10* were PCR amplified from the cDNA library of murine MLL-AF9 cells with primers containing a FLAG. *Hoxa9* cDNA was amplified from pTRE rtTA FLAG HoxA9 GFP[36]. Catalytic mutant HBO1 E508Q was generated by site-directed mutagenesis. Wildtype and mutant Hbo1 were made resistant to sgHbo1 e12.2 by silent point mutation of the PAM site corresponding this sgRNA by site-directed mutagenesis. All cDNAs were cloned into the lentiviral pHRSIN-P_{SFFV}-GFP-P_{PGK}-Puro vector[37]. LSC expressing Cas9 were transduced with expression vectors and selected with 5 μg ml^{-1} puromycin for one week. Overexpression lines were then subsequently transduced with Hbo1 sgRNA.

Animal details

All animal work was performed at the Peter MacCallum Cancer Centre animal facility, under approval E530 from the Peter MacCallum Cancer Centre animal ethics committee and at the Walter and Eliza Hall Institute of Medical Research with approval from the Walter and Eliza Hall Institute Animal Ethics Committee under approval 2015.015. Mx1-Cre *Hbo1*$^{flox/flox}$ mice[10] and *Moz*$^{+/-}$ mice were as previously described[30].

***In vivo* Competition Assay**

6° MLL-AF9 cells were transduced with non-targeting (NT), shHbo1 or shMoz hairpins at 90% transduction efficiency. 100 000 cells were transplanted 48 h post-transduction into 8 week old female NSG mice. BFP positive hairpin positive cells were determined by flow cytometry.

Leukaemia Maintenance

The generation of *Mx1-Cre Hbo1*$^{fl/fl}$ conditional knockout mice have been previously described[10]. c-kit positive cells from whole bone marrow were selected through magnetic bead selection (Miltenyi Biotec) and retrovirally transduced with the MSCV-MLL-AF9-IRES-YFP construct. Cells were transplanted in sublethally irradiated 6-8 week-old female C57BL/6 recipients. 100 000 leukaemic cells from the bone marrow was collected and subsequently transplanted into sublethally irradiated 11-week-old female C57BL/6 recipients. Polyinosinic:polycytidylic (pIpC, GE) was i.p. administered 6, 10, 14 days post-transplantation at 7.5 mg/kg. Amplification of wildtype and floxed alleles of leukaemic cells from bone marrow has been previously described[10].

RNA sequencing and analysis

RNA from sgRNA positive cells was prepared using the Qiagen RNeasy kit. RNA concentration was quantified with a NanoDrop spectrophotometer (Thermo

Scientific). Libraries were prepared using QuantaSeq 3' mRNA Library Prep kit (Lexogen). Libraries were sequenced on a NextSeq500 with 75 bp single end reads. All RNA-seq experiments were performed in triplicate. Following trimming of poly-A tails with cutadapt[38] (v.1.14). Reads were aligned to the mouse genome (ensembl_GRC38.78) using hisat2[39], and assigned to genes using htseq-count[40]. Differential gene expression analysis was performed using the edgeR[41] package in R (http://www.R-project.org/), adjusted *p*-values were calculated using the Benjamini-Hochberg method.[42] Genes with log fold-changes below -1 and adjusted *p*-values below 0.05 were considered to be significantly down-regulated genes. Count data was voom-transformed using the voom function before performing gene set testing with the mroast function[43], both from the limma package[44].

Chromatin immunoprecipitation sequencing (ChIP-seq) and analysis

10-20 million sgRNA positive cells were cross-linked with 1% formaldehyde for 10 min at room temperature and cross-linking was quenched by addition of 0.125 M glycine. Cells then lysed in 1% SDS, 10 mM EDTA, 50 mM Tris-HCl pH 8.0 and protease inhibitors. Lysates were sonicated in a Covaris ultrasonicator to achieve a mean DNA fragment size of 500 bp. Immunoprecipitation with anti-H3K14Ac (Cell Signalling Technolgies) or anti-RNA polymerase II (Millipore) was performed overnight at 4°C in modified RIPA buffer (10 mM Tris-HCl pH 8.0, 90 mM NaCl, 1% Triton X-100, 0.1% deoxycholate). Protein A or G magnetic beads (Life Technologies) were used to bind antibody and associated chromatin. Reverse crosslinking of DNA was followed by DNA purification using the QIAquick PCR purification kit (Qiagen). Sequencing libraries were prepared from eluted DNA using ThruPLEX DNA-seq kit (Rubicon). Libraries were size selected between 200-500 bp and sequenced on a NextSeq500 with 75 bp single end reads. Following the removal of Illumina adaptors using cutadapt[38]. Reads were aligned to a joint reference genome of mouse (ensemble_GRCh38.78) and drosophila (ensemble_BDGP5.78) with bwa-mem (v. 0.7.13). SAM files were converted to BAM files using samtools[45] (v. 1.4.1). A scaling factor was calculated using the drosophila spike-in, as previously described[46]. The scaling factor was used to normalise the coverage across the genome, when calculated using *bamCoverage* from deepTools[47] (v. 2.5.3) with binsizes of 10 bp and filtered with ENCODE project ChIP blacklist regions for mm10 (https://www.encodeproject.org/annotations/ENCSR636HFF/). Genome-browser images were generated from the conversion of BAM files to TDF using igvtools[48] (v. 2.3.95). Heatmap plots were generated using deepTools[47] over the region, 5 kb upstream to 5 kb downstream of the genebody of all genes. Coverage across the length of the genebody was scaled to 5 kb, and regions with no coverage were excluded from the plot.

qRT-PCR

RNA from sgRNA positive cells 4-5 days post-transduction or cells treated with WM-3835 for 6-12 h was extracted using the Qiagen RNAeasy kit. cDNA was prepared using SuperScript VILO (Life Technologies) according to manufacturer's instructions. Quantitative real-time PCR was performed on an Applied Biosystems StepOnePlus using Fast SYBR green reagents (Thermo Scientific). Expression levels were determined using the ΔΔCt method normalised to β2-microglobulin. All mRNA primer sequences are provided in Supplementary Table 3.

Cell Proliferation Assays

Cells were seeded at a constant density prior to treatment in triplicate and treated with either 1 μM WM-3835, 1 μM WM-2474 or DMSO (0.1%) over the indicated time period. Drug was refreshed at least every two days. Cells were stained with DAPI and live cell number was calculated using the BD FACSVerse (BD Biosciences). To determine the IC50 for the WM-3835, four hours after seeding the cells at a constant density in duplicate, they were treated with WM-3835, DMSO or positive control (3 μM puromycin) for 10 days. Drug and media were refreshed at day 4 and 7. At day 10, after incubating the cells with 600 μM of resazurin for 6 h, fluorescence was measured at λex 530 nm and λem 590 nm, using a Microplate Reader (EnSpire, Perkin Elmer). Relative fluorescence units were converted to percent of inhibition relative to controls on the same plate and the data fitted against a four-parameter logistic model to determine the 50% inhibitory concentration (IC50).

Clonogenic Assays in Methylcellulose

Clonogenic potential was assessed through colony growth of AML patient bone marrow plated in cytokine-supplemented methylcellulose (MethoCult H4434, Stemcell Technologies). Bone marrow was plated in duplicate at a cell dose of 2 X 10^4 cells per plate in the presence of vehicle (0.1% DMSO) or 1 μM WM-3835. Cells were incubated at 37°C and 5% CO_2 for 12 days at which time colonies were counted.

Patient Material

Bone marrow containing >80% blasts was obtained from patients following consent and under full ethical approval by the Peter MacCallum Cancer Centre Research Ethics Committee (Reference number: HREC/17/PMCC/69).

Lysine acetyltransferase biochemical assays

KAT enzymes were either produced or purchased as previously described[25]. Lysine acetyltransferase assays were run as described previously[25] with two modification. Firstly, 100 nM of full-length biotinylated histone H3 (for MOZ, QKF, HBO1) or histone H4 (for KAT5, KAT8) proteins were used as the substrate,

as indicated. Secondly, assays were run with 1 μM acetyl-coA concentration, the approximate K_m for acetyl-coA for these enzymes in this assay format.

HBO1 H3K14ac biomarker assay

The cell line U2OS was seeded at a density of 3,000 cells per well in 384-well optical quality tissue culture plates in RPMI medium supplemented with 10% foetal bovine serum and 10 mM HEPES. The cells were allowed to adhere for 24 hours under standard culture conditions (37°C, 5% CO_2). At the end of this period the cells were washed with medium. Compound dilutions prepared in DMSO were added to the medium, with negative control wells reserved for treatment with DMSO only and 100% inhibition positive controls at 10 μM concentration. After incubation for 24 hours, the cells were fixed with 4% formaldehyde in PBS for 15 minutes at room temperature, washed with phosphate buffer saline and blocked with blocking buffer containing 0.2% TritonX100 and 2% BSA. Anti-H3K14ac antibody (Cell Signalling Technologies) in blocking buffer was added and incubated overnight at 4°C. After washing, a secondary antibody labelled with AlexaFluor 488 dye (ThermoFisher) and Hoechst 33342 (1 μg/mL, Life Technologies) were added for 2 hours incubation at room temperature. Plates were washed and read on a PerkinElmer Opera HCS high content imaging platform. Using a Columbus image analysis pipeline, individual nuclei were located by Hoechst 33342 stain and the level of H3K14ac was calculated from the AlexaFluor 488-related intensity in the same area. The resulting mean intensity per cell was converted to percent inhibition relative to controls on the same plate and the data fitted against a four-parameter logistic model to determine the 50% inhibitory concentration (IC50).

HBO1-BPRF2 protein production, SPR, and structural biology

HBO1-BPRF2 protein was produced as described previously[49]. SPR for WM-3835 was done as described[25]. HBO1-BPRF2 protein was produced as described previously[49]. SPR for WM-3835 was done as described[25]. Crystals were grown at the CSIRO C3 crystallisation centre in SD2 sitting drop plates at 20 °C with equal volumes of protein and crystallant (200 nL plus 200 nL drops) with the reservoir consisting of 244 mM diammonium tartrate and 20% PEG 3350. Crystals started to form overnight and were harvested 3 days later using 20% glycerol as a cryoprotectant. Data were obtained at the MX2 microfocus beamline at the Australian Synchrotron. The space group was found to be H3 and the data and refinement statistics can be found in Extended Data Fig. 6. The data were indexed with DIALS[50] (WM-3835) or XDS[51] (acetyl-CoA), scaled and integrated with Aimless[52], the structure was solved with Phaser[53] using PDB entry 5GK9 as the initial model, manual refined with Coot[54] and full refinement was done with Phenix.refine[55] (WM-3835) or REFMAC[56] (acetyl-CoA). Crystal structure data for HBO1-BPRF2 in complex with WM-3835 and acetyl-CoA have been submitted to the Protein Data Bank (PDB) under accession numbers 6MAJ (WM-3835) and

6MAK (acetyl-CoA). Crystallisation and refinement statistics are shown in Extended Data Fig. 10.

In vitro metabolic stability

The metabolic stability assay was performed by incubating each test compound in liver microsomes at 37 °C and a protein concentration of 0.4 mg/mL. The metabolic reaction was initiated by the addition of either single cofactor (NADPH only), or dual cofactors (NADPH and UDPGA), and quenched at various time points over a 60-minute incubation period by the addition of acetonitrile containing diazepam as internal standard. Control samples (containing no NADPH) were included (and quenched at 2, 30 and 60 minutes) to monitor for potential degradation in the absence of cofactor. The human liver microsomes used in this experiment were supplied by XenoTech, lot # 1410230. The mouse liver microsomes used in this experiment were supplied by XenoTech, lot # 1510256. Microsomal incubations were performed at a substrate concentration of 1 μM.

Code availability

All code used in this study are publically available and are detailed in the method section.

Data availability

The shRNA screen sequencing data have been deposited to the NCBI Sequence Archieve under the accession number GSE120813. Source Data are provided for Figs 1, 2, 3, 4.

Supplementary References:

26. Gilan, O. *et al.* Functional interdependence of BRD4 and DOT1L in MLL leukemia. *Nat Struct Mol Biol* **23**, 673-81 (2016).
27. Cancer Genome Atlas Research, N. *et al.* Genomic and epigenomic landscapes of adult de novo acute myeloid leukemia. *N Engl J Med* **368**, 2059-74 (2013).
28. Bagger, F.O. *et al.* BloodSpot: a database of gene expression profiles and transcriptional programs for healthy and malignant haematopoiesis. *Nucleic Acids Res* **44**, D917-24 (2016).
29. Majewski, I.J. *et al.* Polycomb repressive complex 2 (PRC2) restricts hematopoietic stem cell activity. *PLoS Biol* **6**, e93 (2008).
30. Voss, A.K., Collin, C., Dixon, M.P. & Thomas, T. Moz and retinoic acid coordinately regulate H3K9 acetylation, Hox gene expression, and segment identity. *Dev Cell* **17**, 674-86 (2009).
31. Kinkel, S.A. *et al.* Jarid2 regulates hematopoietic stem cell function by acting with polycomb repressive complex 2. *Blood* **125**, 1890-900 (2015).
32. Keniry, A. *et al.* Setdb1-mediated H3K9 methylation is enriched on the inactive X and plays a role in its epigenetic silencing. *Epigenetics Chromatin* **9**, 16 (2016).
33. Dai, Z. *et al.* edgeR: a versatile tool for the analysis of shRNA-seq and CRISPR-Cas9 genetic screens. *F1000Res* **3**, 95 (2014).
34. Shechter, D., Dormann, H.L., Allis, C.D. & Hake, S.B. Extraction, purification and analysis of histones. *Nat Protoc* **2**, 1445-57 (2007).
35. Cox, J. & Mann, M. MaxQuant enables high peptide identification rates, individualized p.p.b.-range mass accuracies and proteome-wide protein quantification. *Nat Biotechnol* **26**, 1367-72 (2008).
36. Brumatti, G. *et al.* HoxA9 regulated Bcl-2 expression mediates survival of myeloid progenitors and the severity of HoxA9-dependent leukemia. *Oncotarget* **4**, 1933-47 (2013).
37. Tchasovnikarova, I.A. *et al.* GENE SILENCING. Epigenetic silencing by the HUSH complex mediates position-effect variegation in human cells. *Science* **348**, 1481-1485 (2015).
38. Martin, M. Cutadapt removes adapter sequences from high-throughput sequencing reads. *2011* **17**, 3 (2011).
39. Kim, D., Langmead, B. & Salzberg, S.L. HISAT: a fast spliced aligner with low memory requirements. *Nat Methods* **12**, 357-60 (2015).
40. Lavallee, V.P. *et al.* The transcriptomic landscape and directed chemical interrogation of MLL-rearranged acute myeloid leukemias. *Nat Genet* **47**, 1030-7 (2015).
41. Ritchie, M.E. *et al.* limma powers differential expression analyses for RNA-sequencing and microarray studies. *Nucleic Acids Res* **43**, e47 (2015).
42. Benjamini, Y. & Hochberg, Y. Controlling the False Discovery Rate: A Practical and Powerful Approach to Multiple Testing. *Journal of the Royal Statistical Society. Series B (Methodological)* **57**, 289-300 (1995).
43. Wu, D. *et al.* ROAST: rotation gene set tests for complex microarray experiments. *Bioinformatics* **26**, 2176-82 (2010).

44. Robinson, M.D., McCarthy, D.J. & Smyth, G.K. edgeR: a Bioconductor package for differential expression analysis of digital gene expression data. *Bioinformatics* **26**, 139-40 (2010).
45. Li, H. *et al.* The Sequence Alignment/Map format and SAMtools. *Bioinformatics* **25**, 2078-9 (2009).
46. Orlando, D.A. *et al.* Quantitative ChIP-Seq normalization reveals global modulation of the epigenome. *Cell Rep* **9**, 1163-70 (2014).
47. Ramirez, F. *et al.* deepTools2: a next generation web server for deep-sequencing data analysis. *Nucleic Acids Res* **44**, W160-5 (2016).
48. Robinson, J.T. *et al.* Integrative genomics viewer. *Nat Biotechnol* **29**, 24-6 (2011).
49. Tao, Y., Zhong, C., Zhu, J., Xu, S. & Ding, J. Structural and mechanistic insights into regulation of HBO1 histone acetyltransferase activity by BRPF2. *Nucleic Acids Res* **45**, 5707-5719 (2017).
50. Waterman, D.G. *et al.* Diffraction-geometry refinement in the DIALS framework. *Acta Crystallogr D Struct Biol* **72**, 558-75 (2016).
51. Kabsch, W. Xds. *Acta Crystallogr D Biol Crystallogr* **66**, 125-32 (2010).
52. Evans, P.R. & Murshudov, G.N. How good are my data and what is the resolution? *Acta Crystallogr D Biol Crystallogr* **69**, 1204-14 (2013).
53. McCoy, A.J. *et al.* Phaser crystallographic software. *J Appl Crystallogr* **40**, 658-674 (2007).
54. Emsley, P., Lohkamp, B., Scott, W.G. & Cowtan, K. Features and development of Coot. *Acta Crystallogr D Biol Crystallogr* **66**, 486-501 (2010).
55. Afonine, P.V. *et al.* Towards automated crystallographic structure refinement with phenix.refine. *Acta Crystallogr D Biol Crystallogr* **68**, 352-67 (2012).
56. Murshudov, G.N., Vagin, A.A. & Dodson, E.J. Refinement of macromolecular structures by the maximum-likelihood method. *Acta Crystallogr D Biol Crystallogr* **53**, 240-55 (1997).

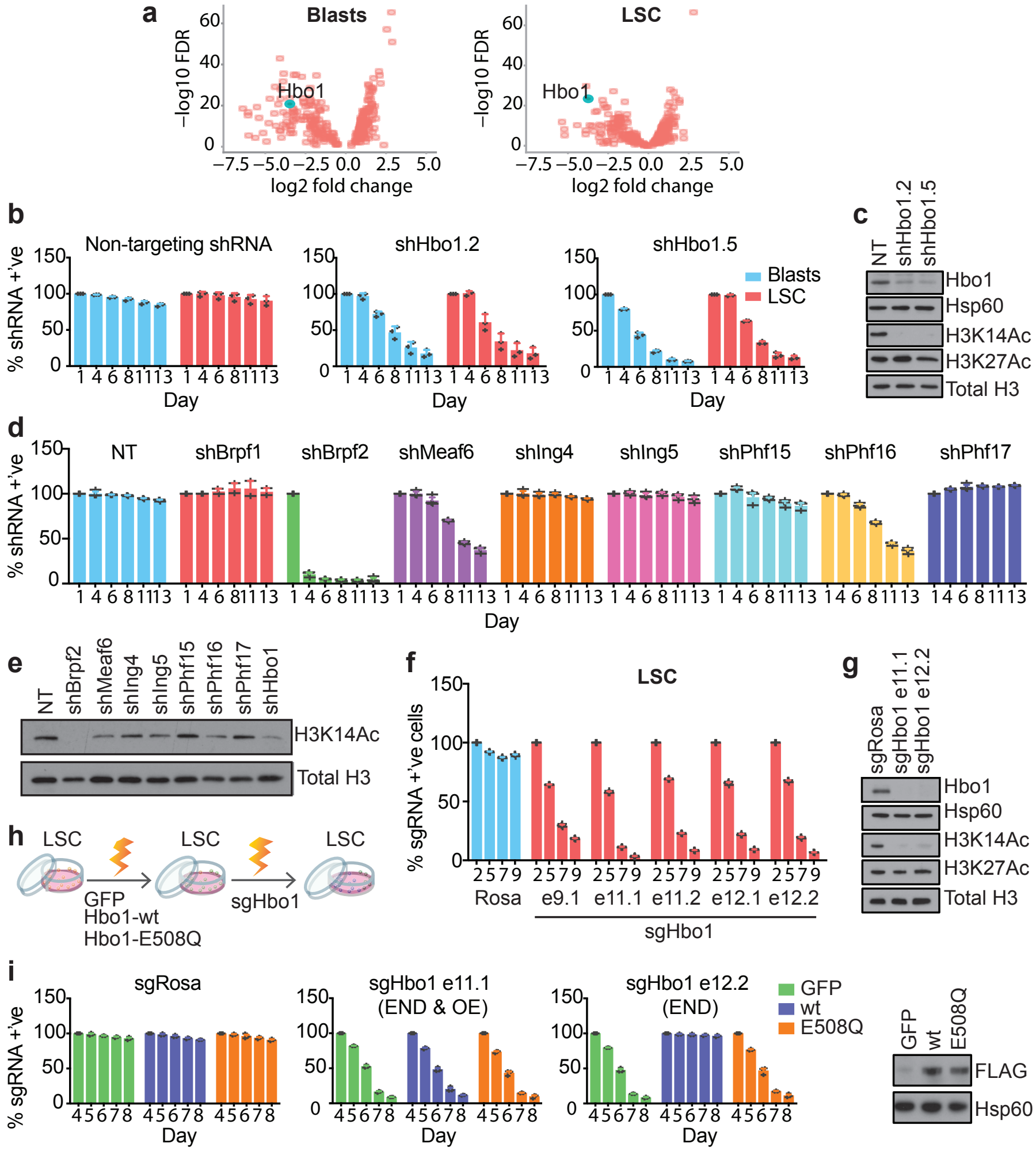
a
Blasts
LSC
−log10 FDR
Hbo1
log2 fold change
b
Non-targeting shRNA
shHbo1.2
shHbo1.5
% shRNA +'ve
Day
Blasts
LSC
c
NT
shHbo1.2
shHbo1.5
Hbo1
Hsp60
H3K14Ac
H3K27Ac
Total H3
d
NT
shBrpf1
shBrpf2
shMeaf6
shIng4
shIng5
shPhf15
shPhf16
shPhf17
% shRNA +'ve
Day
e
NT
shBrpf2
shMeaf6
shIng4
shIng5
shPhf15
shPhf16
shPhf17
shHbo1
H3K14Ac
Total H3
f
LSC
% sgRNA +'ve cells
Rosa
e9.1
e11.1
e11.2
e12.1
e12.2
sgHbo1
g
sgRosa
sgHbo1 e11.1
sgHbo1 e12.2
Hbo1
Hsp60
H3K14Ac
H3K27Ac
Total H3
h
LSC
LSC
LSC
GFP
Hbo1-wt
Hbo1-E508Q
sgHbo1
i
sgRosa
sgHbo1 e11.1
(END & OE)
sgHbo1 e12.2
(END)
% sgRNA +'ve
Day
GFP
wt
E508Q
FLAG
Hsp60

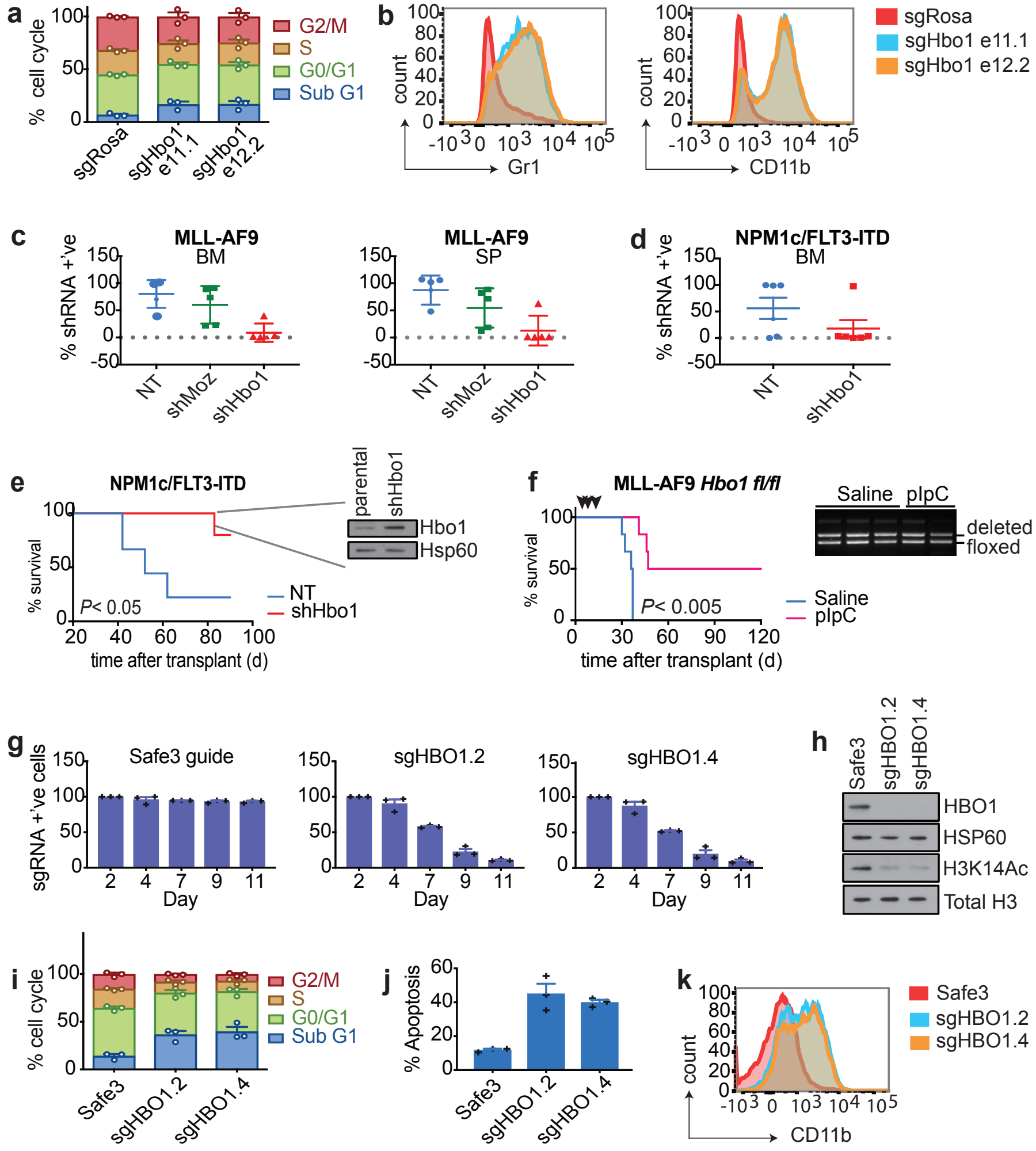
a
% cell cycle
G2/M
S
G0/G1
Sub G1
sgRosa
sgHbo1 e11.1
sgHbo1 e12.2
b
count
Gr1
CD11b
sgRosa
sgHbo1 e11.1
sgHbo1 e12.2
c
MLL-AF9
BM
SP
% shRNA +'ve
NT
shMoz
shHbo1
d
NPM1c/FLT3-ITD
BM
e
NPM1c/FLT3-ITD
% survival
P< 0.05
time after transplant (d)
parental
shHbo1
Hbo1
Hsp60
f
MLL-AF9 Hbo1 fl/fl
P< 0.005
time after transplant (d)
Saline
pIpC
deleted
floxed
g
sgRNA +'ve cells
Safe3 guide
sgHBO1.2
sgHBO1.4
Day
h
Safe3
sgHBO1.2
sgHBO1.4
HBO1
HSP60
H3K14Ac
Total H3
i
% cell cycle
G2/M
S
G0/G1
Sub G1
Safe3
sgHBO1.2
sgHBO1.4
j
% Apoptosis
k
count
CD11b
Safe3
sgHBO1.2
sgHBO1.4

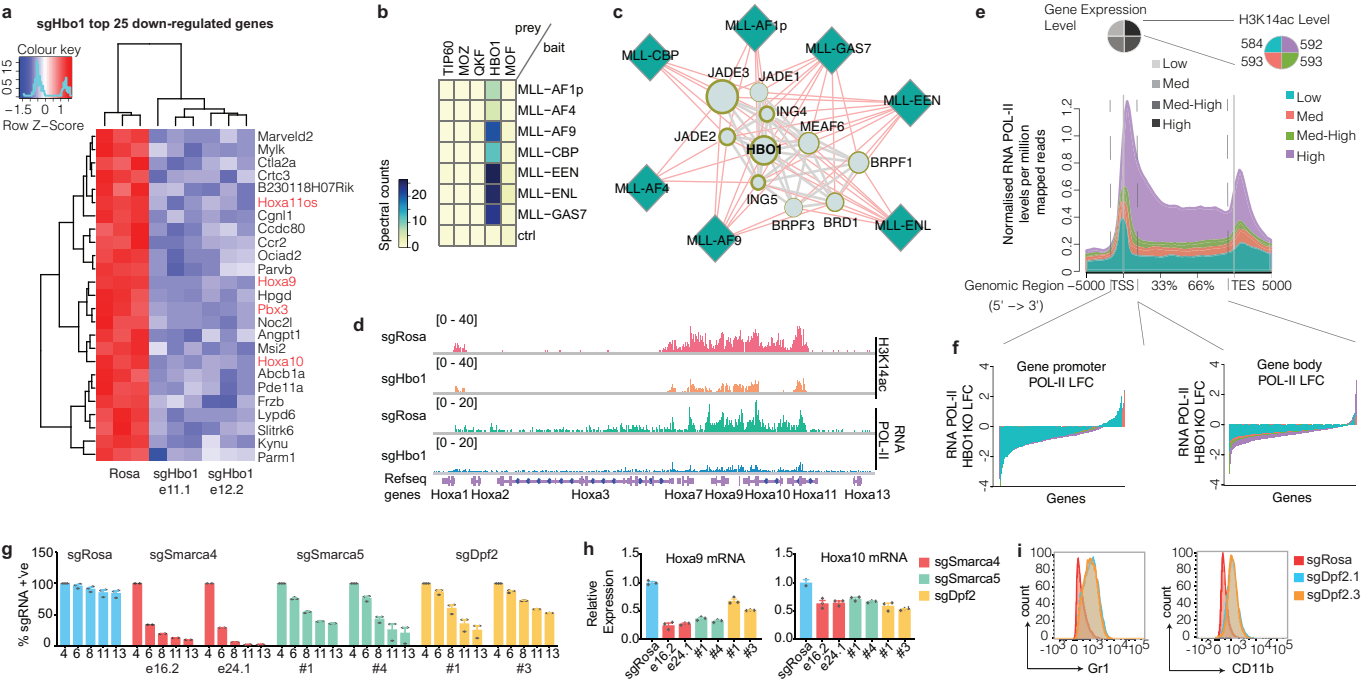
a
sgHbo1 top 25 down-regulated genes
Colour key
0.5 1.5
−1.5 0 1
Row Z−Score
Marveld2
Mylk
Ctla2a
Crtc3
B230118H07Rik
Hoxa11os
Cgnl1
Ccdc80
Ccr2
Ociad2
Parvb
Hoxa9
Hpgd
Pbx3
Noc2l
Angpt1
Msi2
Hoxa10
Abcb1a
Pde11a
Frzb
Lypd6
Slitrk6
Kynu
Parm1
Rosa
sgHbo1 e11.1
sgHbo1 e12.2
b
prey
bait
TIP60
MOZ
QKF
HBO1
MOF
MLL−AF1p
MLL−AF4
MLL−AF9
MLL−CBP
MLL−EEN
MLL−ENL
MLL−GAS7
ctrl
Spectral counts
20
10
0
c
MLL-AF1p
MLL-CBP
MLL-GAS7
JADE3
JADE1
MLL-EEN
ING4
JADE2
MEAF6
HBO1
BRPF1
MLL-AF4
ING5
BRPF3
BRD1
MLL-ENL
MLL-AF9
d
sgRosa
[0 - 40]
sgHbo1
[0 - 40]
H3K14ac
sgRosa
[0 - 20]
sgHbo1
[0 - 20]
RNA POL-II
Refseq genes
Hoxa1 Hoxa2
Hoxa3
Hoxa7 Hoxa9 Hoxa10 Hoxa11
Hoxa13
e
Gene Expression Level
H3K14ac Level
584
592
593
593
Low
Med
Med-High
High
Low
Med
Med-High
High
Normalised RNA POL-II levels per million mapped reads
0
0.2
0.4
0.6
0.8
1.0
1.2
Genomic Region
−5000
TSS
33%
66%
TES
5000
(5' −> 3')
f
Gene promoter POL-II LFC
RNA POL-II HBO1KO LFC
Genes
Gene body POL-II LFC
RNA POL-II HBO1KO LFC
Genes
g
% sgRNA +ve
150
100
50
0
sgRosa
sgSmarca4
sgSmarca5
sgDpf2
4 6 8 11 13
e16.2
e24.1
#1
#4
#1
#3
h
Hoxa9 mRNA
Hoxa10 mRNA
Relative Expression
1.5
1.0
0.5
0.0
sgRosa
e16.2
e24.1
#1
#4
#1
#3
sgSmarca4
sgSmarca5
sgDpf2
i
100
80
60
40
20
0
count
−10^3 0 10^3 10^4 10^5
Gr1
CD11b
sgRosa
sgDpf2.1
sgDpf2.3

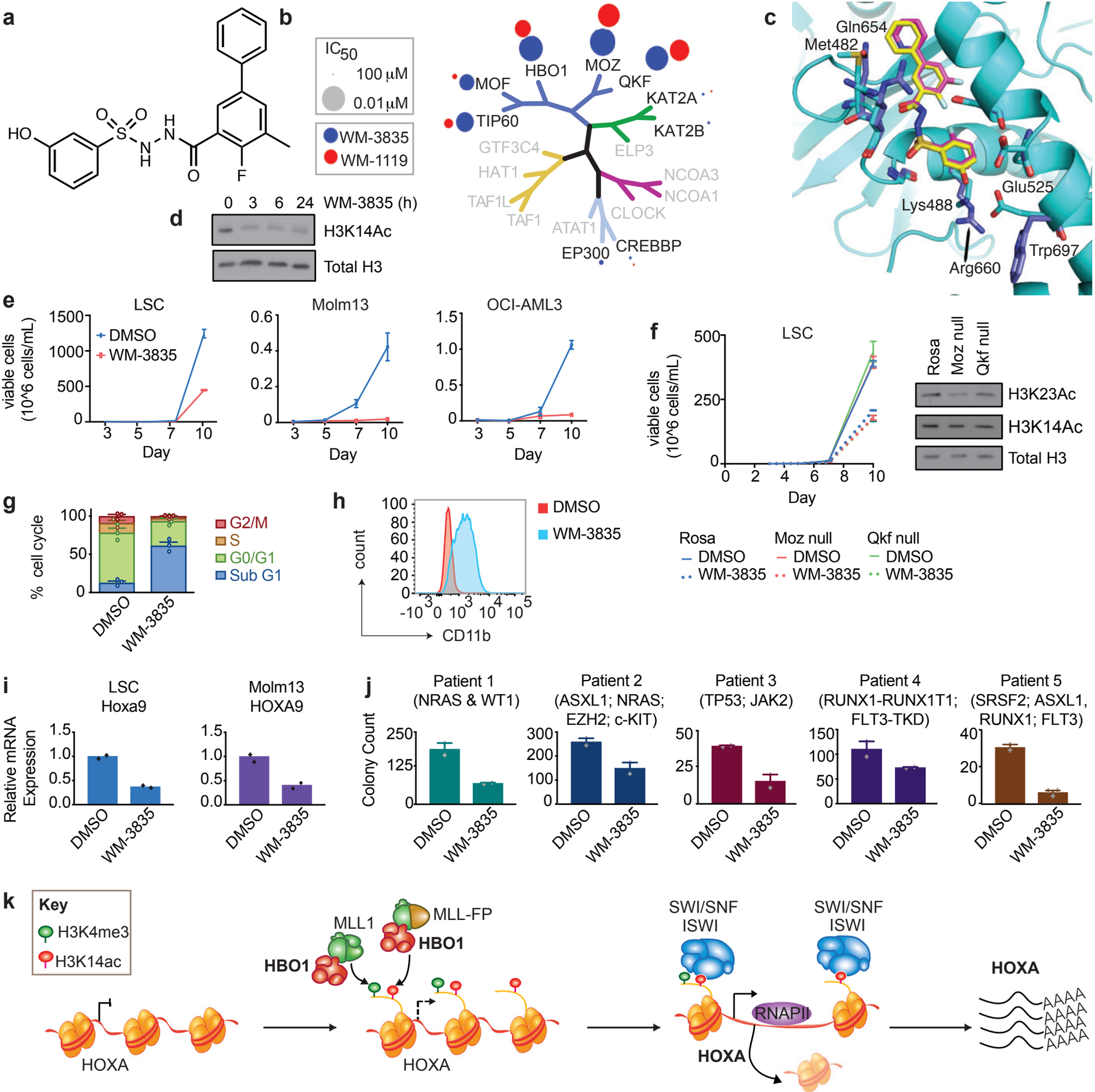
a
HO
O
S
O
N
H
N
H
O
F
b
IC50
100 μM
0.01 μM
WM-3835
WM-1119
HBO1
MOZ
MOF
QKF
KAT2A
TIP60
KAT2B
GTF3C4
ELP3
HAT1
NCOA3
NCOA1
TAF1L
CLOCK
TAF1
ATAT1
EP300
CREBBP
c
Gln654
Met482
Glu525
Lys488
Trp697
Arg660
d
0 3 6 24 WM-3835 (h)
H3K14Ac
Total H3
e
LSC
Molm13
OCI-AML3
viable cells (10^6 cells/mL)
DMSO
WM-3835
Day
f
LSC
viable cells (10^6 cells/mL)
Day
Rosa
Moz null
Qkf null
H3K23Ac
H3K14Ac
Total H3
g
% cell cycle
G2/M
S
G0/G1
Sub G1
DMSO
WM-3835
h
count
CD11b
DMSO
WM-3835
Rosa
Moz null
Qkf null
i
LSC Hoxa9
Molm13 HOXA9
Relative mRNA Expression
j
Patient 1 (NRAS & WT1)
Patient 2 (ASXL1; NRAS; EZH2; c-KIT)
Patient 3 (TP53; JAK2)
Patient 4 (RUNX1-RUNX1T1; FLT3-TKD)
Patient 5 (SRSF2; ASXL1, RUNX1; FLT3)
Colony Count
k
Key
H3K4me3
H3K14ac
MLL1
MLL-FP
HBO1
HOXA
SWI/SNF
ISWI
RNAPII
HOXA